Direct observation of spin excitation anisotropy in the paramagnetic orthorhombic state of $BaFe_{2-x}Ni_{x}As_{2}$

Haoran Man, Rui Zhang, J. T. Park, Xingye Lu, J. Kulda, A. Ivanov, and Pengcheng Dai

Phys. Rev. B **97**, 060507 — Published 21 February 2018

DOI: 10.1103/PhysRevB.97.060507

Direct observation of spin excitation anisotropy in the paramagnetic orthorhombic state of $BaFe_{2-x}Ni_xAs_2$

Haoran Man,[1] Rui Zhang,[1] J. T. Park,[2] Xingye Lu,[3] J. Kulda,[4] A. Ivanov,[4] and Pengcheng Dai[1,3,*]

[1]*Department of Physics and Astronomy, Rice University, Houston, Texas 77005, USA*
[2]*Heinz Maier-Leibnitz Zentrum, TU München, Lichtenbergstraße 1, D-85747 Garching, Germany*
[3]*Center for Advanced Quantum Studies and Department of Physics, Beijing Normal University, Beijing 100875, China*
[4]*Institut Laue-Langevin, 71 avenue des Martyrs, 38000 Grenoble, France*

(Dated: February 6, 2018)

We use transport and inelastic neutron scattering measurements to investigate single crystals of iron pnictide $BaFe_{2-x}Ni_xAs_2$ ($x = 0, 0.03$), which exhibit a tetragonal-to-orthorhombic structural transition at T_s and stripe antiferromagnetic order at T_N ($T_s \geq T_N$). Using a tunable uniaxial pressure device, we detwin the crystals and study their transport and spin excitation properties at antiferromagnetic wave vector $S_1(1, 0)$ and its 90° rotated wave vector $S_2(0, 1)$ under different pressure conditions. We find that uniaxial pressure necessary to detwin and maintain single domain orthorhombic antiferromagnetic phase of $BaFe_{2-x}Ni_xAs_2$ induces resistivity and spin excitation anisotropy at temperatures above zero pressure T_s. In uniaxial pressure-free detwinned sample, spin excitation anisotropy between $S_1(1, 0)$ and $S_2(0, 1)$ first appear in the paramagnetic orthorhombic phase below T_s. These results are consistent with predictions of spin nematic theory, suggesting the absence of structural or nematic phase transition above T_s in iron pnictides.

In the phase diagrams of high-temperature superconductors, there are many exotic ordered phases which break spatial symmetries of the underlying lattice in addition to superconductivity[1]. One such phase is the electronic nematic phase which breaks orientational, but not translational, symmetry of the underlying lattice[2]. For iron pnictides such as $BaFe_{2-x}Ni_xAs_2$[3,4], there exists a structural transition at T_s, where the crystal structure changes from tetragonal to orthorhombic, followed by an antiferromagnetic (AF) transition at temperature T_N slightly below T_s ($T_N \leq T_s$)[5,6]. In the paramagnetic state above T_N, there are ample evidence for an electronic nematic phase from transport[7–12], magnetic torque[13], shear-modulus[14], scanning tunneling microscopy (STM)[15,16], angle resolved photoemission spectroscopy (ARPES)[17], nuclear magnetic resonance (NMR)[18,19], and neutron scattering experiments[20–24]. In particular, transport[7–12], ARPES[17], and neutron scattering[20,22–24] experiments on single crystals of iron pnictides reveal that the nematic phase first appears below a characteristic temperature T^* above T_s and T_N, where the system is in the paramagnetic tetragonal state. The nematic phase has been suggested as a distinct phase at T^* well above T_s[13]. Theoretically, it has been argued that the experimentally observed electronic nematic phase is due to spin[25–29] or orbital[30,31] degrees of freedom, and should only appear in the paramagnetic orthorhombic phase below T_s.

To understand this behavior, we note that iron pinctides exhibiting tetragonal-to-orthorhombic structural transition form twin domains below T_s due to small mismatch of the lattice constants of the orthorhombic axes (a and b) in the FeAs plane[16]. To unveil the intrinsic electronic properties of the system, an external uniaxial pressure (stress) must be applied along the in-plane orthorhombic axis, forcing the short b-axis to align with the external pressure, and drive the twinned domain sample into a single domain suitable for electronic anisotropy measurements[9]. Although an externally applied uniaxial pressure can effectively change the twin-domain population, it also introduces an artificial anisotropic strain field that breaks the four fold rotational symmetry of the paramagnetic tetragonal phase and induces an orthorhombic lattice distortion in iron pnictides above T_s[23]. While transport, neutron diffraction, and Raman scattering measurements carried out under tunable uniaxial pressure on single crystals of iron pnictides suggest that resistivity anisotropy found above T_s in transport measurements[7–12,14] is likely induced by the external pressure[32,33], much is still unclear concerning the nature of the nematic phase and its microscopic origin. In particular, if the electronic nematic phase has a spin origin, one would expect that spin excitation anisotropy at the AF ordering wave vector $\mathbf{Q}_{AF} = S_1(1, 0)$ and 90° rotated wave vector $S_2(0, 1)$ first appears below T_s with increasing spin-spin correlations at $S_1(1, 0)$ and decreasing spin-spin correlations at $S_2(0, 1)$ (Fig. 1)[27,28]. Although recent inelastic neutron scattering experiments confirm the increasing spin-spin correlations at $S_1(1, 0)$ and decreasing spin-spin correlations at $S_2(0, 1)$ in electron-doped iron pnictide $BaFe_{1.935}Ni_{0.065}As_2$, the measurements were carried out under an uniaxial pressure and spin excitation anisotropy first appears at a temperature well above T_s[24]. Therefore, it is still unclear if spin excitation anisotropy above T_s is induced by the applied uniaxial pressure or an intrinsic property of the spin nematic phase in iron pnictide.

Our $BaFe_{2-x}Ni_xAs_2$ ($x = 0, 0.03$) single crystals were grown using self-flux method [Fig. 1(a)][34]. The crystal orientations were determined by X-ray Laue machine, and the square-shaped samples were cut for neutron scattering and transport measurements. All samples were

annealed at 800 K for 2 days to reduce defects and disorder. Transport measurements were carried out using a physical property measurement system (PPMS). We used the standard four-probe method and measured resistivity on warming with a slow rate. The in-plane resistivity anisotropy was measured using Montgomery method as described before[32]. By taking the first derivative of the resistivity data in $BaFe_{1.97}Ni_{0.03}As_2$ [Fig. 4(f)], we can see clear split of T_N and T_s, with $T_N \approx 109$ K and $T_s \approx 113$ K.

Using a specially designed tunable uniaxial pressure device[32], we study spin excitations at $S_1(1,0)$ and $S_2(0,1)$, and resistivity anisotropy in single domain orthorhombic $BaFe_{2-x}Ni_xAs_2$ [Fig. 1(a)]. The nematic order parameter can be obtained by comparing the dynamic spin-spin correlation function $S(\mathbf{Q},\omega)$ at $\mathbf{Q}_{AF} = S_1(1,0)$ and $\mathbf{Q}_2 = S_2(0,1)$ in the paramagnetic orthorhombic ($T_s > T > T_N$) and tetragonal ($T > T_s$) phases [Figs. 1(b)-(d)][28]. In the stress-free state, one expects that the differences in $S(\mathbf{Q},\omega)$ at $S_1(1,0)$ and $S_2(0,1)$ would only occur below T_s [Figs. 1(c) and (d)][28]. By measuring $S(\mathbf{Q},\omega)$ at $\mathbf{Q}_{AF}$ and $\mathbf{Q}_2 = S_2$ and comparing the outcome with transport measurements under different uniaxial pressure in $BaFe_{2-x}Ni_xAs_2$, we find that applied uniaxial pressure indeed induces spin excitation anisotropy above T_s, and such anisotropy only appears below T_s in the stress-free sample, consistent with theoretical prediction[28]. Our transport and inelastic neutron scattering experiments thus reveal a direct correlation between spin excitation and resistivity anisotropy, suggesting that resistivity anisotropy and associated nematic phase has a spin origin[25–29].

We designed an in-situ mechanical device which can apply and release uniaxial pressure at any temperature below 300 K [Fig. 1(e)][32]. With a micrometer on top, the magnitude of the uniaxial pressure along the b-axis of the orthorhombic lattice is controlled by a spring compressed by the displacement of the micrometer. By applying pressure at room temperature ($\gg T_s$), cooling sample down below T_N, and releasing the pressure, we can measure the intrinsic electronic properties of iron pnictides in the AF ordered state without external pressure (stress-free). Three types of measurements are carried out:

1. Pressure applied: unaixial pressure sufficient to detwin the sample is applied during the entire measurement. Both intrinsic and pressure induced effect will contribute to measured transport and spin excitation anisotropy.

2. Pressure released: a uniaxial pressure is applied on cooling from room temperature to base temperature ($\ll T_N$). The pressure is then released at base temperature. Transport and spin excitation measurements were carried out on warming, where the sample remains partially detwinned and only intrinsic electronic difference in the orthorhombic state contribute to measured transport and spin excitation anisotropy.

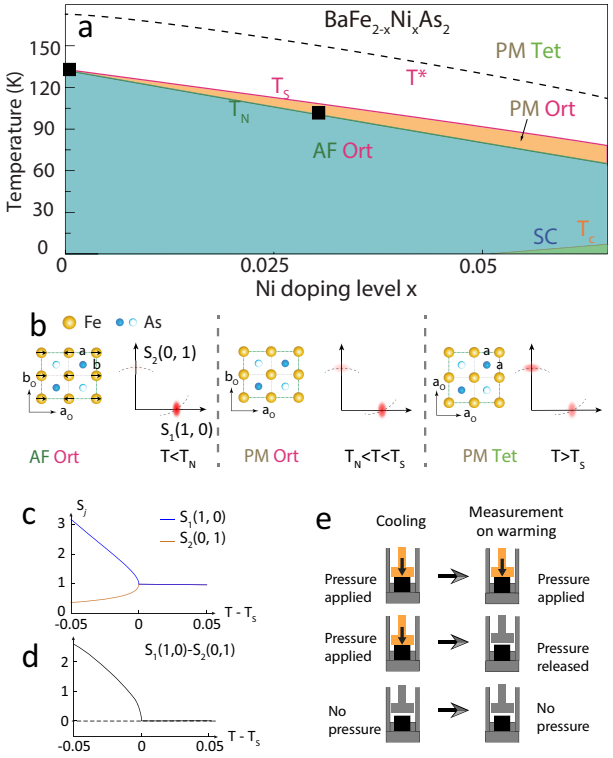

FIG. 1: (a) The electronic phase diagram of $BaFe_{2-x}Ni_xAs_2$ as a function of Ni-doping as determined from previous work[6]. The AF orthorhombic (AF Ort), paramagnetic orthorhombic (PM Ort), paramagnetic tetragonal (PM Tet), and superconductivity (SC) phases are clearly marked. Black square points mark the Ni-doping levels measured in this paper. (b) Schematic illustration of Fe-As layer at different temperatures and its corresponding reciprocal space for temperature $T < T_N$, $T_N > T > T_s$, and $T > T_s$. The AF ordering wave vector and its 90° rotation are marked as $S_1(1,0)$ and $S_2(0,1)$, respectively. The dotted curves are in-plane projection of neutron scattering scan trajectories in reciprocal space. (c) Temperature dependence of the spin-spin correlation length at $S_1(1,0)$ (blue) and $S_2(0,1)$ (orange) across T_s as predicted by spin nematic theory[28]. (d) The corresponding temperature dependence of the magnetic intensity difference between $S_1(1,0)$ and $S_2(0,1)$. (e) Schematic diagrams of the in-situ device used to change pressure on the sample. A micrometer and a spring are used to adjust the pressure applied to the sample[32]. The applied pressure can be released by a full retreat of the micrometer, leaving the sample partially detwinned at low temperature.

3. No Pressure: No uniaxial pressure is applied to the sample and the sample remains in the twinned state below T_s and T_N. If twin domains are equally distributed, there should be no transport and spin excitation anisotropy.

Our inelastic neutron scattering experiments were carried out at the IN-8 triple-axis spectrometer using a multi-analyzer detector system, Institut Laue-Langevin (ILL), Grenoble, France[35]. For inelastic neutron scat-

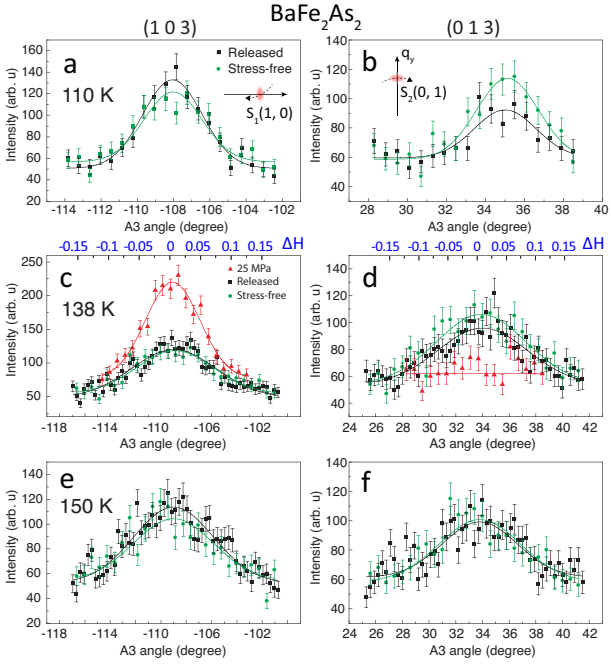

FIG. 2: Inelastic neutron scattering measurements of 10 meV spin excitations of $BaFe_2As_2$ under different conditions at $S_1(1,0)$ and $S_2(0,1)$. Transverse A3 (rocking) scans at different temperature and pressure conditions. The corresponding wave vector directions in reciprocal space are shown in the insets of (a) and (b). The scans are measured under 25 MPa pressure (red), pressure released (black), and stress-free (green) cases. (a,b) at 110 K ($< T_N/T_s$); (c,d) 138 K ($\approx T_N/T_s$); (e,f) 150 K ($> T_N/T_s$).

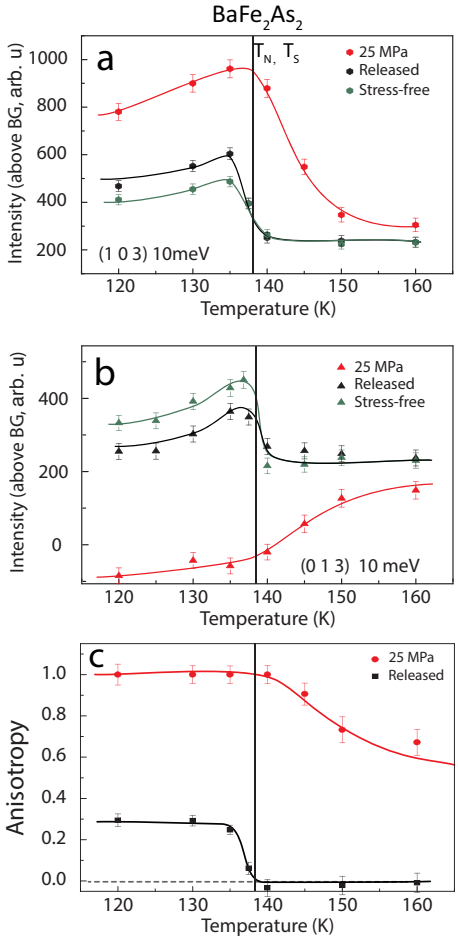

FIG. 3: Temperature dependence of spin excitations at 10 meV in $BaFe_2As_2$ under 25 MPa uniaxial pressure, pressure released, and stress-free conditions at (a) AF wave vector $S_1(1,0) = (1,0,3)$; (b) $S_1(0,1) = (0,1,3)$. The negative scattering is due to imperfect background scattering subtraction. (c) Temperature dependence of spin excitation anisotropy under 25 MPa pressure and pressure-released.

tering experiments, annealed square-shaped single crystals of $BaFe_2As_2$ (~220 mg) or $BaFe_{1.97}Ni_{0.03}As_2$ (~200 mg) were mounted on the sample stick specially designed for applying uniaxial pressure (along b-axis) inside an orange cryostat[32]. The momentum transfer $\mathbf{Q}$ in three-dimensional reciprocal space in Å^{-1} is defined as $\mathbf{Q} = H\mathbf{a}^* + K\mathbf{b}^* + L\mathbf{c}^*$, where H, K, and L are Miller indices and $\mathbf{a}^* = \hat{\mathbf{a}}2\pi/a$, $\mathbf{b}^* = \hat{\mathbf{b}}2\pi/b$, $\mathbf{c}^* = \hat{\mathbf{c}}2\pi/c$ with $a \approx b \approx 5.549$ Å and $c \approx 12.622$ Å[6]. In the AF ordered state of a fully detwinned sample, the AF Bragg peaks occurs at $(\pm 1, 0, L)$ $(L = 1, 3, 5, \cdots)$ positions in reciprocal space and are absent at $(0, \pm 1, L)$. The sample was aligned in the $[H, 0, L]$ scattering plane. With goniometer below the orange cryostat and with extra coverage provided by the flat-cone setup on IN8[35], we can access both $(1, 0, 3)$ and $(0, 1, 3)$ around 10 meV and $(1, 0, 5)$, $(0, 1, 5)$ magnetic Bragg peak positions at 0 meV.

We have collected neutron scattering data under three different conditions: (1) under 22-25 MPa uniaxial pressure (pressured); (2) pressure released at 10 K and no pressure measurements on warming (released); and (3) no pressure at all temperatures (stress-free) [Figure 1(e)]. For each scenario, spin excitations at wave vectors $(1, 0, 3)$ and $(0, 1, 3)$ are measured in the same warm-up cycle. We first test if spin excitation anisotropy seen above T_N/T_s in uniaxial pressured $BaFe_2As_2$[20] also exists in pressure released situation. Figures 2(a) and 2(b) compare transverse scans of spin excitations at 10 meV and 110 K ($< T_N$) for pressure released and stress-free cases at wave vectors $S_1(1, 0)$ and $S_2(0, 1)$, respectively. Assuming spin excitations are isotropic in stress-free situation, we find clear spin excitation anisotropy in pressure released situation, consistent with previous elastic scattering measurements below T_N[32]. On warming to 138 at T_N/T_s, spin excitations in the pressured case double that of the stress-free case and only exist at $S_1(1, 0)$, consistent with a fully pressure-induced detwinned state [Figs. 2(c) and 2(d)][20]. For comparison, transverse scans in pressure released and stress-free cases are indistinguishable. Upon further warming up to 150 K above T_N/T_s, we again find no spin excitation anisotropy at $S_1(1, 0)$

and $S_2(0,1)$ [Figs. 2(e) and 2(f)], suggesting that spin excitation anisotropy only appears below T_N/T_s in pressure released case.

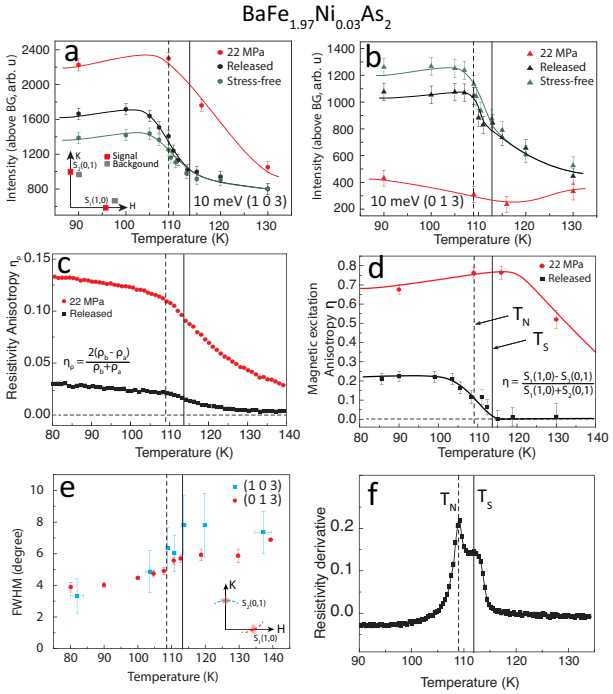

FIG. 4: Temperature dependence of resistivity and spin excitations anisotropy for $BaFe_{1.97}Ni_{0.03}As_2$. (a) Temperature dependence of the 10 meV spin excitations under 22 MPa, released, and stress-free conditions at $S_1(1,0)$. (b) Similar measurements at $S_2(0,1)$. Temperature dependence of the (c) resistivity and, (d) spin excitation anisotropy under 22 MPa and pressure released conditions. (e) Temperature dependence of the FWHM of the 10 meV spin excitations at $S_1(1,0)$ and $S_2(0,1)$. The scan directions are marked by dotted curve in the inset. (f) Temperature dependence of the first derivative of resistivity, where T_N and T_s are marked as vertical lines.

To confirm these results, we carried out spin excitation measurements in these three pressure conditions using long counting time at the peak center and subtracted background points. Figures 3(a) and 3(b) show the background subtracted peak intensities at $S_1(1,0) = (1,0,3)$ and $S_2(0,1) = (0,1,3)$, respectively. In case one under 25 MPa uniaxial pressure (red), the large spin excitation anisotropy at $S_1(1,0)$ and $S_2(0,1)$ below T_N/T_s persists to temperatures well above T_N/T_s, consistent with earlier results[20]. For case two pressure released measurements (black), while the spin excitation anisotropy between $S_1(1,0) = (1,0,3)$ and $S_2(0,1) = (0,1,3)$ becomes much smaller compared with stress-free case, it is still present below 138 K but vanishes above 138 K at both wave vectors. By normalizing pressured and released data with stress-free measurements at $S_1(1,0)$ and $S_2(0,1)$, we can estimate the spin excitations anisotropy η using $\eta = (I_{(1,0)} - I_{(0,1)})/(I_{(1,0)} + I_{(0,1)})$, where $I_{(1,0)}$ and $I_{(0,1)}$ are spin excitations at $S_1(1,0)$ and $S_2(0,1)$, respectively. For a fully detwinned sample in the stress-free AF ordered state, only $I_{(1,0)}$ should be present and $\eta = 1$. In the stress-free paramagnetic tetragonal state, we expect $I_{(1,0)} = I_{(0,1)}$ and $\eta = 0$. Figure 3(c) indicates that uniaxial pressure is necessary to maintain 100% detwinned state in $BaFe_2As_2$. While spin excitations still have anisotropy in the pressured released case below T_N/T_s, the anisotropy completely vanishes above T_N/T_s. These measurements confirm that spin excitation anisotropy above T_N/T_s are entirely induced by externally applied uniaxial pressure.

Having established the vanishing spin excitation anisotropy in the paramagnetic state of $BaFe_2As_2$, where $T_N \approx T_s$ without applied uniaxial pressure, it is interesting to ask if spin excitations can be anisotropic in the stress-free paramagnetic orthorhombic nematic phase as predicted by spin nematic theory[25–29]. For this experiment, we chose $BaFe_{1.97}Ni_{0.03}As_2$ because of its separated T_N and T_s ($> T_N$) [Fig. 4(f)][6]. Figures 4(a) and 4(b) show temperature dependence of the magnetic scattering at 10 meV for $S_1(1,0) = (1,0,3)$ and $S_2(0,1) = (0,1,3)$, respectively. Similar to measurement on $BaFe_2As_2$, spin excitation anisotropy under 22 MPa uniaxial pressure (red) extends to temperatures well above T_s [Figs. 4(a),(b),(d)]. However, the pressure released data (black) is much closer to stress-free data on approaching T_s. For temperature above T_s, there are no detectable differences between $S_1(1,0)$ and $S_2(0,1)$, as seen in Fig. 4(d). Therefore, spin excitations exhibit a weak anisotropy in the paramagnetic orthorhombic phase of $BaFe_{1.97}Ni_{0.03}As_2$, consistent with theoretical expectation for a spin excitation driven nematic phase[25–29]. For comparison, Figure 4(c) shows temperature dependence of the resistivity anisotropy obtained under 22 MPa uniaxial pressure (red) and pressure released (black) conditions. For pressure released case, we find no evidence of time dependent relaxation of the resistivity anisotropy within several hours. Although resistivity anisotropy reduces dramatically in the pressure released case, it is still present in a narrow temperature region above T_s and below ~130 K, due possibly to the residual anisotropic strain in the sample [4(c)][32]. Since increasing uniaxial pressure enhances both the resistivity and spin excitation anisotropy, there must be a direct correlation between the resistivity and spin excitation anisotropy.

To further test if spin-spin correlation length also increases at $S_1(1,0)$ but decreases at $S_2(0,1)$ below T_s as expected from the spin nematic theory[27–29] [Fig. 1(c)][27,28], we show in Fig. 4(e) temperature dependence of the full-width-half-maximum (FWHM) of spin excitations at 10 meV along the marked scan directions at $S_1(1,0)$ and $S_2(0,1)$. At both wave vectors, we find a clear reduction of the FWHM in spin excitations around T_s. However, since the data collected at $S_2(0,1)$ is along the transverse direction, we cannot directly compare the outcome with spin nematic theory, which predicted an increase in spin-spin excitation correlation length mea-

surable for scans along the longitudinal direction.

In summary, by using a specially designed in-situ detwinning device to tune the applied uniaxial pressure, we study spin excitation and resistitivity anisotropy in AF order and paramagnetic phases of $BaFe_{2-x}Ni_xAs_2$. For undoped parent compound $BaFe_2As_2$ with $T_N \approx Ts$, we find clear spin excitation anisotropy in the pressure released AF ordered phase at 10 meV, but anisotropy vanishes in the paramagnetic tetragonal phase. For pressure released electron-doped $BaFe_{1.97}Ni_{0.03}As_2$ with $T_N < T_s$, the spin excitation anisotropy at 10 meV present in the AF ordered phase decreases on warming, persists in the paramagnetic orthorhombic phase ($> T_N$) before vanishing in the paramagnetic tetragonal state above T_s. Assuming the small resistivity anisotropy above T_s in pressure released sample is extrinsic effect due to residual strain, our results establish a direct correlation between spin excitation and resistivity anisotropy, and are consistent with predictions of spin nematic theory[25–29]. Therefore, our data indicate no additional phase transition above T_s, and suggest that the observed resistivity anisotropy in the paramagnetic tetragonal phase[7–12] arises from strong magnetoelastic coupling due to the presence of strong nematic fluctuations.

We are grateful to Sebastien Turc, E. Bourgeat-Lami, E. Lelièvre-Berna of ILL, France for designing and constructing the detwinning device used at IN8. The neutron scattering work at Rice is supported by the U.S. NSF Grant No. DMR-1700081 (P.D.). The $BaFe_{2-x}Ni_xAs_2$ single-crystal synthesis work at Rice is supported by the Robert A. Welch Foundation Grant No. C-1839 (P.D.).

* Electronic address: pdai@rice.edu

1 B. Keimer, S. A. Kivelson, M. R. Norman, S. Uchida, S., and J. Zaanen, Nature **518**, 179-186 (2015)‘.

2 E. Fradkin, S. A. Kivelson, M. J. Lawler, J. P. Eisenstein, and A. P. Mackenzie, Annu. Rev. Condens. Matter Phys. **1**, 153 (2010).

3 G. R. Stewart, Reviews of Modern Physics **83**, 1589-1652 (2011).

4 P. C. Dai, Reviews of Modern Physics **87**, 855-896 (2015).

5 H. Luo, R. Zhang, M. Laver, Z. Yamani, M. Wang, X. Lu, M. Wang, Y. Chen, S. Li, S. Chang, J. W. Lynn, P. C. Dai, Phys. Rev. Lett. **108**, 247002 (2012).

6 X. Lu, H. Gretarsson, R. Zhang, X. Liu, H. Luo, W. Tian, M. Laver, Z. Yamani, Y. -J. Kim, A. H. Nevidomskyy, Q. Si, and P. C. Dai, Phys. Rev. Lett. **110**, 257001 (2013).

7 J. H. Chu *et al.*, Science **329**, 824 (2010).

8 M. A. Tanatar, E. C. Blomberg, A. Kreyssig, M. G. Kim, N. Ni, A. Thaler, S. L. Bud'ko, P. C. Canfield, A. I. Goldman, I. I. Mazin, and R. Prozorov, Phys. Rev. B **81**, 814508 (2010).

9 I. R. Fisher, L. Degiorgi, L., and Z. X. Shen, Rep. Prog. Phys. **74**, 124506 (2011).

10 J. H. Chu, H. -H. Kuo, J. G. Analytis, I. R. Fisher, Science **337**, 710 (2012).

11 H.-H Kuo, M. C. Shapiro, S. C. Riggs, I. R. Fisher, Phys. Rev. B **88**, 085113 (2013).

12 H. -H. Kuo, J. -H. Chu, S. A. Kivelson, and I. R. Fisher, Science **352**, 958 (2016).

13 S. Kasahara, H. J. Shi, K. Hashimoto, S. Tonegawa, Y. Mizukami, T. Shibauchi, K. Sugimoto, T. Fukuda, T. Terashima, A. H. Nevidomskyy, and Y. Matsuda, Nature **486**, 382 (2012).

14 A. E. Böhmer and C. & Meingast, C. R. Phys. **17**, 90 (2016).

15 E. P. Rosenthal, E. F. Andrade, C. J. Arguello, R. M. Fernandes, L. Y. Xing, X. C. Wang, C. Q. Jin, A. J. Millis, A. N. Pasupathy, Nat. Phys. **10**, 225 (2014).

16 C. Cantoni, M. A. McGurie, B. Sparov, A. F. May, T. Keiber, F. Bridges, A. S. Sefat, and B. C. Sales, Adv. Mater. **27**, 2715-2721(2015).

17 M. Yi, Y. Zhang, Z.-X. Shen, and D. H. Lu, NPJ Quantum Materials **2**, 57 (2017).

18 M. Fu, D. A. Torchetti, T. Imai, F. L. Ning, J.-Q. Yan, and A. S. Sefat, Phys. Rev. Lett. **109**, 247001 (2012).

19 A. P. Dioguardi, T. Kissikov, C. H. Lin, K. R. Shirer, M.M. Lawson, H.-J. Grafe, J.-H. Chu, I. R. Fisher, R.M. Fernandes, and N. J. Curro, Phys. Rev. Lett. **116**, 107202 (2016).

20 X. Y. Lu, J. T. Park, R. Zhang, H. Q. Luo, A. H. Nevidomskyy, Q. Si, and P. C. Dai, Science **345**, 657 (2014).

21 Q. Zhang, R. M. Fernandes, J. Lamsal, J. Yan, S. Chi, G. S. Tucker, D. K. Pratt, J.W. Lynn, R. McCallum, P. C. Canfield, T. A. Lograsso, A. I. Goldman, D. Vaknin, and R. J. McQueeney, Phys. Rev. Lett. **114**, 057001 (2015).

22 Y. Song, X. Lu, D. L. Abernathy, D.W. Tam, J. L. Niedziela, W. Tian, H. Luo, Q. Si, and P. Dai, Phys. Rev. B **92**, 180504(R) (2015).

23 X. Lu, K.-F. Tseng, T. Keller,W. Zhang, D. Hu, Y. Song, H. Man, J. T. Park, H. Luo, S. Li, , Phys. Rev. B **93**, 134519 (2016).

24 W. L. Zhang, J. T. Park, X. Y. Lu, Y. Wei, X. Ma, L. Hao, P. C. Dai, Z. Meng, Y. F. Yang, H. Luo, and S. Li, Phys. Rev. Lett. **117**, 227003 (2016).

25 C. Fang, H. Yao, W.-F. Tsai, J. P. Hu, and S. A. Kivelson, Phys. Rev. B **77**, 224509 (2008).

26 C. Xu, M. Muller, and S. Sachdev, Phys. Rev. B 78, 020501 (2008).

27 R. M. Fernandes, A. V. Chubukov, and J. Schmalian, Nat. Phys. **10**, 97 (2014).

28 R. M. Fernandes and J. Schmalian, Supercond. Sci. Technol. **25**, 084005 (2012).

29 S. Liang, A. Moreo, and E. Dagotto, Phys. Rev. Lett. **111**, 047004 (2013).

30 C.-C. Lee, W.-G. Yin, and W. Ku, Phys. Rev. Lett. **103**, 267001 (2009).

31 W. Lv, J.Wu, and P. Phillips, Phys. Rev.B **80**, 224506 (2009).

32 Haoran Man, Xingye Lu, Justin S. Chen, Rui Zhang, Wenliang Zhang, Huiqian Luo, J. Kulda, A. Ivanov, T. Keller, Emilia Morosan, Qimiao Si, and Pengcheng Dai. Phys. Rev. B **92**, 134521 (2015).

33 Xiao Ren, Lian Duan, Yuwen Hu, Jiarui Li, Rui Zhang, Huiqian Luo, Pengcheng Dai, and Yuan Li Phys. Rev. Lett. **115**, 197002 (2015).

34 Y. C. Chen, X. Y. Lu, M. Wang, H. Q. Luo, and S. L. Li,

Supercond. Sci. Technol. **24**, 065004 (2011).
[35] J. Kulda, Nuclear Engineering and Technology **38**, 433 (2006).